

X-ray absorption and rapid variability of the dwarf Seyfert nucleus of NGC4395

K. Iwasawa¹, A.C. Fabian¹, O. Almaini², P. Lira^{2,3}, A. Lawrence²,
K. Hayashida⁴ and H. Inoue⁵

¹*Institute of Astronomy, Madingley Road, Cambridge CB3 0HA*

²*Institute for Astronomy, University of Edinburgh, Royal Observatory, Blackford Hill, Edinburgh EH9 3HJ*

³*Department of Physics and Astronomy, University of Leicester, University Road, Leicester, LE1 7RH*

⁴*Department of Earth and Space Science, Osaka University, Machikaneyama, Toyonaka, Osaka 560-0043, Japan*

⁵*Institute of Space and Astronautical Science, Yoshinodai, Sagamihara, Kanagawa 229-8510, Japan*

ABSTRACT

We report the detection of an absorbed central X-ray source and its strong, rapid, variability in NGC4395, the least luminous Seyfert nucleus known. The X-ray source exhibits a number of flares with factors of 3–4 flux changes during a half day ASCA observation. The shortest doubling time observed is about 100 s. Such X-ray variability is in contrast to the behaviour of other low luminosity active galaxies and resembles that of higher luminosity Seyfert 1 galaxies. It provides further support for an accreting black hole model rather than an extreme stellar process in accounting for the nuclear activity of NGC4395. The ASCA spectrum shows a power-law continuum of photon-index $\Gamma = 1.7 \pm 0.3$ with a Fe K line marginally detected at ~ 6.4 keV. The soft X-ray emission below 3 keV is strongly attenuated by absorption. The energy spectrum in this absorption band shows a dramatic change in response to the variation in continuum luminosity. A variable warm absorber appears to be the most likely explanation to account for the spectral change. The absorption-corrected 2–10 keV luminosity is $4 \times 10^{39} \text{ erg s}^{-1}$ for a source distance of 2.6 Mpc, and at 1 keV is one order of magnitude above previous ROSAT estimates, which affects the appearance of the wide-band spectral energy distribution and photoionization calculations. The rapid X-ray variation is consistent with a black hole of a few times $10^4 M_{\odot}$, as suggested by the optical results and the small bulge of this dwarf galaxy. Such a light black hole is favoured also in order for the Eddington ratio ($L_{\text{Bol}}/L_{\text{Edd}}$) to be above the range of ADAFs, which would clearly fail to explain the observed X-ray variability. The nuclear source of NGC4395 is therefore consistent with a scaled-down version of higher luminosity Seyfert nuclei, with an intermediate mass (10^4 – $10^5 M_{\odot}$) black hole, unlike the nearby low luminosity active galaxies in which underfed massive black holes are suspected to reside.

Key words: Galaxies: individual: NGC4395 — Galaxies: Seyfert — X-rays: galaxies

1 INTRODUCTION

Recent kinematical studies of nearby galaxies have shown that massive dark objects (MDOs) appear to be ubiquitous at the centre of galaxies (e.g. Kormendy & Richstone 1995), and that most luminous galaxies seem to have MDOs, most likely black holes, with mass ranging 10^6 – $10^9 M_{\odot}$ (e.g., Richstone et al 1998). Many of these objects are, however, significantly underluminous relative to the estimated gas supply (e.g. Fabian & Rees 1995). To account for this,

the Advection-Dominated Accretion Flow (ADAF) solutions relevant for low accretion rates have been proposed.

Recent extensive optical spectroscopic surveys (e.g., Ho, Filippenko & Sargent 1997a) have revealed that a fair fraction of nearby galaxies exhibit some level of activity in their nuclei. Their optical spectra typically show LINER (Heckman 1980) properties and broad H α emission is seen in some of them (Ho, Filippenko & Sargent 1997b). Whether these low activity objects are scaled-down versions of more luminous Seyfert 1 and QSO nuclei or an alternative mechanism is responsible is an important issue.

Such low luminosity active galactic nuclei (dwarf AGN) tend to show weak X-ray variability compared with the higher luminosity Seyfert 1 galaxies investigated by Nandra et al (1997). Ptak et al (1998) interpreted this as evidence for ADAFs operating at low accretion rate in dwarf AGN.

NGC4395 hosts one of the dwarf Seyfert nuclei in the Ho et al (1997a,b) sample, and the least luminous AGN known. This dwarf galaxy is a late-type spiral of low surface brightness with no significant bulge. A study of stellar kinematics indicates a shallow gravitational potential of the small bulge ($< 8 \times 10^4 M_{\odot}$, Filippenko & Ho 2000) and hence the central black hole (e.g., Magorrian et al 1998). Similarly small black hole masses ($\sim 10^5 M_{\odot}$) have been estimated from optical investigations of the active nucleus (Lira et al 1999; Kraemer et al 1999).

A point-like optical nucleus located in the centre of the galaxy shows emission-line properties more resembling a Seyfert 1 nucleus than a LINER (Filippenko & Sargent 1989; Filippenko, Ho & Sargent 1993). Ho et al (1997a) classified NGC4395 as a Seyfert 1.8 on account of the presence of broad permitted line emission ($\text{FWZI}(\text{H}\alpha) \sim 5000 \text{km s}^{-1}$) and high excitation condition. A number of coronal lines like $[\text{FeVII}]\lambda 6087$, $[\text{FeX}]\lambda 6374$ (e.g., Ho et al 1997b; Kraemer et al 1999) are detected and the broad Balmer emission was found to be variable (Lira et al 1999). The contribution of stellar light to the nuclear spectrum appears to be minimal as no significant absorption lines are seen in the HST UV spectrum (Filippenko, Ho & Sargent 1993), although weak CaIIK absorption was found by Lira et al (1999) who estimate the stellar light contribution to be about 10 per cent in the blue band. The apparent deficit of ionizing photons relative to the observed $\text{H}\beta$ luminosity (e.g., Moran et al 1999), similar to some Seyfert 2 nuclei, indicates that the UV continuum source is attenuated by some obscuration in the line of sight, while the narrow-line region (NLR) seems to be little obscured apart from Galactic extinction ($E(B-V) = 0.017$, Kraemer et al 1999). Electron scattering is suggested as an origin of the optical continuum polarisation (6.7 per cent) reported by Barth, Filippenko & Moran (1999), but the result is also consistent with transmission through aligned dust.

NGC4395 has been observed in X-rays with the ROSAT PSPC and HRI. Lira et al (1999) and Moran et al (1999) independently analyzed the data and found the nuclear X-ray source to vary by a factor of ~ 2 in two weeks. The soft X-ray luminosity is estimated to be $10^{38} \text{erg s}^{-1}$, which led them to interpret the nuclear source as X-ray quiet compared with its wide band spectral energy distribution. We observed NGC4395 in the higher energy X-ray band with ASCA and find that the soft X-ray emission observed with ROSAT is faint due to absorption and the primary X-ray source has a luminosity one order of magnitude above the ROSAT estimate, when corrected for the absorption. We also find the X-ray source to be extremely variable unlike the other dwarf AGN studied by Ptak et al (1998). The properties of the absorber and the central source, assuming an intermediate mass black hole, are discussed on the basis of the X-ray results.

Table 1. The mean count rates of NGC4395 observed with the ASCA four detectors. Values for large (ϕ_{Large}) and small (ϕ_{Small}) apertures are given for the SIS data. See Section 5 for the details of the photon-collection regions. No correction for vignetting and point spread function has been made.

Detector	ϕ_{Large} 10^{-2}ct s^{-1}	ϕ_{Small} 10^{-2}ct s^{-1}
S0	6.5	3.2
S1	4.7	2.7
G2	3.8	—
G3	6.1	—

2 OBSERVATIONS AND DATA REDUCTION

NGC4395 was observed with ASCA on 1998 May 24–25 for a half day. The two Solid state Imaging Spectrometers (SIS; S0 and S1) were operating in 1CCD Faint mode throughout the observation. The best calibrated CCD chip on each detector (S0C1 and S1C3) was used. The field in the vicinity of NGC4395 is remarkably crowded with bright X-ray sources (e.g., see the ROSAT PSPC image by Radecke 1997). The 1CCD mode observation restricted the SIS field of view to a 11×11 arcmin box which covers the nucleus of NGC4395 and four other soft X-ray sources detected with the ROSAT PSPC. The Gas Imaging Spectrometer (GIS; G2 and G3) has a larger field of view (~ 40 arcmin in diameter) in which at least four more X-ray sources are significantly detected. These sources all have soft X-ray counterparts detected with the PSPC (Radecke 1997).

The data reduction was carried out using FTOOLS version 4.2 and standard calibration provided by the ASCA Guest Observer Facility (GOF) at Goddard Space Flight Center. The pointing error of the ASCA satellite induced by the distortion of the base plate of the star tracker has been corrected so that the pointing accuracy in the ASCA images presented in this paper is the order of 10 arcsec. The good exposure time is about 21 ks for each detector. The mean count rates of NGC4395 obtained from the four detectors are summarised in Table 1. Response matrices for the SIS were generated by SISRMG version 1.1. Version 4.0 of the redistribution matrices provided by the GIS team are used for the GIS. The effective areas of the source spectra were computed with ASCAARF version 2.73.

3 X-RAY IMAGES

Five sources have been detected within 3 arcmin from the nucleus of NGC4395 in the ROSAT PSPC image (Moran et al 1999), and we use the same naming convention (A, B, C, D and E) for the five X-ray sources as used by Moran et al (1999, see Fig. 1 in their paper). Since the separations between the sources are not sufficiently large compared to the Point Spread Function (PSF) of the ASCA X-ray Telescope (XRT with the half-power diameter of 3 arcmin, Serlemitsos et al 1995), these sources are resolved more clearly in the ROSAT PSPC image of higher spatial resolution. The position of source A coincides with the optical nucleus of NGC4395. The brightest source E is found to have a distinctly softer spectrum than the other sources.

The three ASCA SIS images in the energy bands of 0.6–

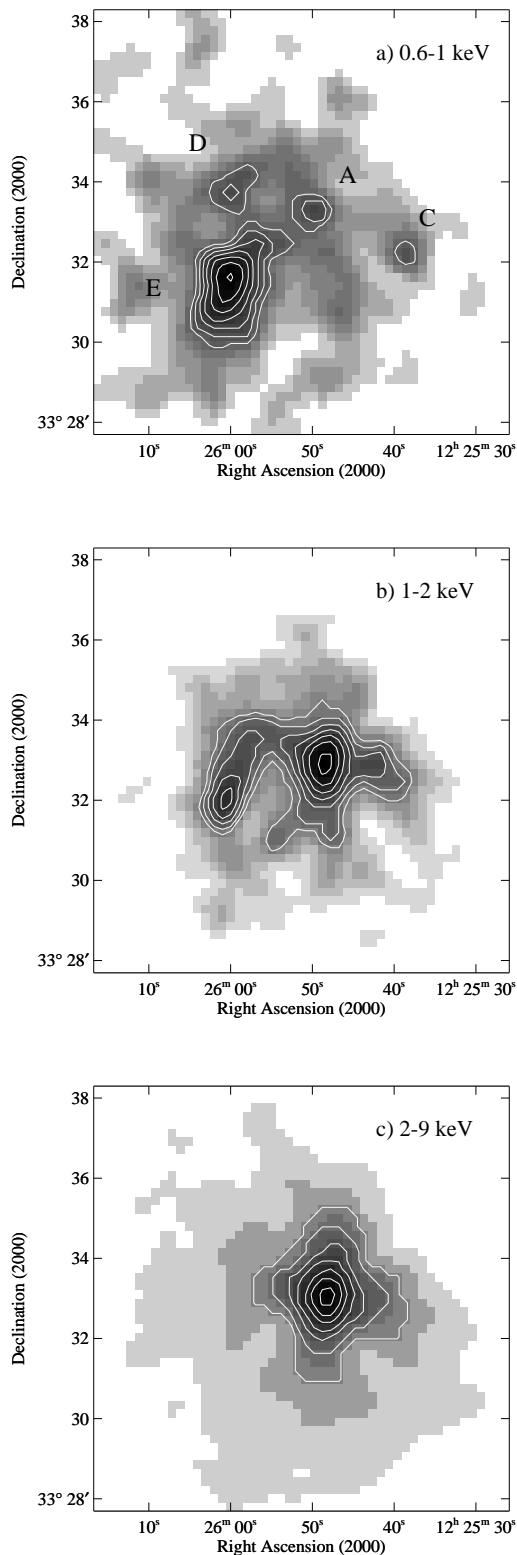


Figure 1. The ASCA SIS images of the NGC4395 region in the energy bands of a) 0.6–1 keV, b) 1–2 keV and c) 2–9 keV. Seven contour levels are drawn, equally spaced in intensity, between the peak and 2σ level of background. The ROSAT PSPC sources, A, C, D and E (see Fig. 1 in Moran et al 1999 for naming convention) are seen in the 0.6–1 keV band. The nuclear source A becomes prominent in the 1–2 keV band and it is the only significant source in the 2–9 keV band.

1 keV, 1–2 keV and 2–9 keV are shown in Fig. 1. The data from the two SIS detectors have been added together. In the 0.6–1 keV band image, all the PSPC sources except for B are seen (B is too faint or unresolved with ASCA). E is the brightest source in the low energy band, as in the PSPC image. However, the nuclear source A becomes brighter than E in the 1–2 keV band. C and D are also visible. Finally, in the 2–9 keV band, A is the only source detected in the field. This indicates that the nuclear source of NGC4395 is bright above the ROSAT band and thus has a hard spectrum. The brightest ROSAT source, E, declines steeply around 2 keV in intensity and emits little X-ray emission above that energy.

4 X-RAY VARIABILITY

4.1 Light curve and timing analysis

The source photons of the SIS are collected from a 6×6 arcmin box centred on source A, excluding a circular region with a radius of 1 arcmin centred on E which is ~ 2.8 arcmin away from A. This photon-collection region still contains B, C and D. Since the exclusion of the central part of the E image discards only 40 per cent of the total photons from E as a result of the broad PSF of the ASCA XRT (Serlemittos et al 1995), about 30 per cent of the photons from E should also spread over the region. We attribute as much as 70 per cent of the observed SIS counts in the 0.6–1 keV band to contamination by examining the ROSAT image in conjunction with the PSF of the ASCA XRT. Since the image analysis shows that the nuclear source of NGC4395 dominates the energy band above 2 keV, the data collected from this region is presumed to be free from contamination in the energy band above 2 keV.

Although the two bright sources, A and E, are resolved in the GIS image, cross contamination between the two sources is severer than for the SIS due to the detector’s poorer spatial resolution. Therefore we used a simple circular region with a radius of 5 arcmin centred on source A, discarding the data below 2 keV.

The 2–10 keV SIS and GIS light curves with 128 s bins are shown in Fig. 2. Those light curves were produced in the same procedure described in Nandra et al (1997) and the two detectors of the same type of instruments are co-added. X-ray flux changes are seen on various time scales from a hundred seconds to half-day of the whole observing run. The shortest doubling time is only ~ 100 s. At least three flares with a duration of ~ 1000 s are seen in a time interval, 3.2×10^4 – 4.3×10^4 s, indicated in Fig. 2 (hereafter this time interval is called “active” state and the rest is “quiescent” state).

We have verified that the position of the brightest X-ray source during the “active” period coincides with the position of source A, or the optical nucleus of NGC4395. This rules out the possibility that one of the nearby X-ray sources is responsible for the X-ray flaring.

The normalized excess variance, σ_{RMS}^2 , was defined in Nandra et al (1997) as a measure of variability amplitude. (Note that Turner et al (1999) have pointed out a mistake in the formula quoted by Nandra et al (1997) for the error on σ_{RMS}^2 . We have used the corrected formula given by Turner

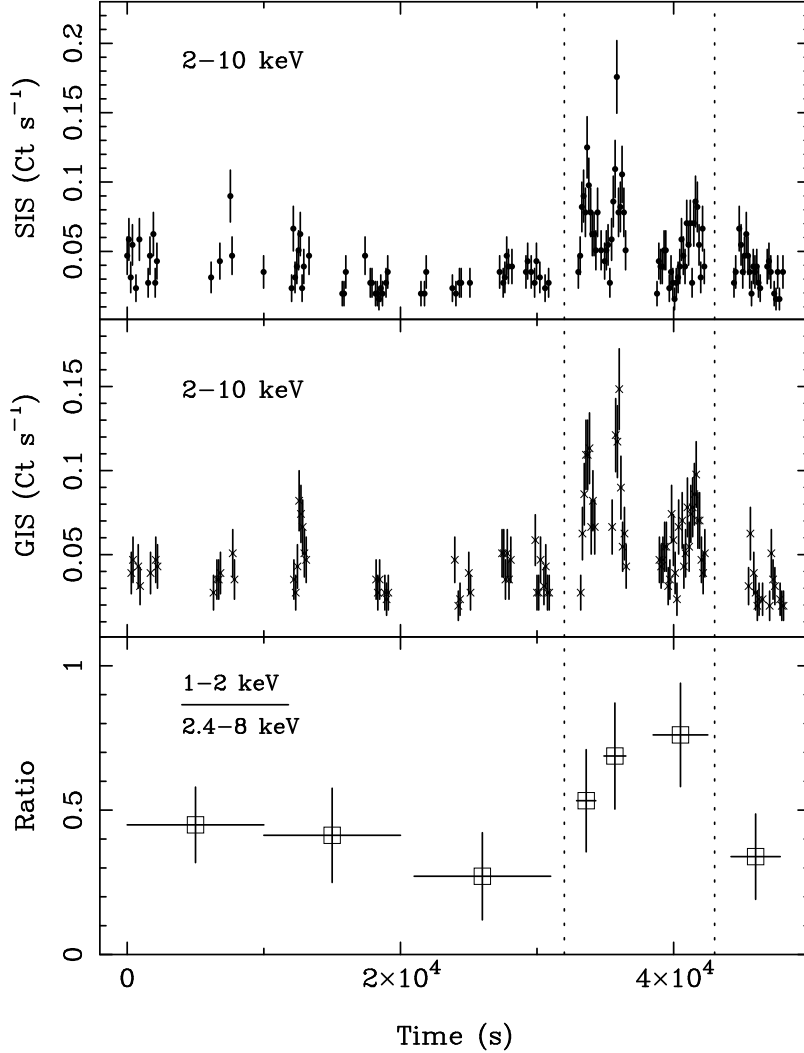


Figure 2. Top and middle panels: the 2–10 keV band light curves of source A in NGC4395 obtained from the ASCA SIS and GIS; bottom panel: the SIS count rate ratio in the 1–2 keV to 2.4–8 keV bands obtained from the small aperture. The epoch of the light curves is 1998 May 24, 16h32m25s (UT). The active phase (3.2×10^4 – 4.3×10^4 s), during which the X-ray source exhibits flares, is indicated in the figure. The mean (1–2 keV)/(2.4–8 keV) count-rate ratios during the active and quiescent phases are 0.66 ± 0.10 and 0.37 ± 0.07 , respectively, showing significant spectral softening during the active phase (see also Fig. 4 and Fig. 5), although a χ^2 test for the data points plotted in the bottom panel does not rule out a constant hypothesis.

et al 1999.) We computed σ_{RMS}^2 for the 2–10 keV light curves and found 0.203 ± 0.066 for the SIS and 0.176 ± 0.047 for the GIS.

Our light curve data are not sufficient to calculate a fully sampled power spectrum by standard means. However we estimate the spectral properties by two methods. First, we estimate the power spectrum using the algorithm of Lomb (1976) which is specially designed for irregularly sampled data. The result shows the red-noise character typical of more luminous AGN. Next, we make a quantitative comparison to other AGN, by calculating the normalized power spectral density (NPSD), following the methodology of Hayashida et al (1998) at a small number of frequencies, which is presented in Fig. 3. The error bars on each data point are too large to constrain the slope of the power spectrum. However the amplitude of variability in NGC4395 is comparable to that of NGC4051 observed with Ginga (Hayashida et al 1998).

4.2 Spectral variability

In order to investigate the soft X-ray spectrum (below 2 keV), data restricted within a small aperture around the nuclear source are taken from the SIS detectors so that the contamination is minimized. A circular region with a 3 arcmin diameter, which corresponds to the half-power diameter of the ASCA XRT PSF, is used instead of the original photon collection region. A contribution from the nearby sources in the band below 1 keV is expected to be about 10 per cent, but should be negligible in the 1–2 keV band.

The count rate ratio in the 1–2 keV to 2.4–8 keV bands obtained from the small aperture SIS data is plotted in Fig. 2. The excess variation in the soft band relative to the hard band is confirmed by the spectral ratio between the active and quiescent states (Fig. 4). The data are consistent with a flux change by a factor of 2 with no spectral variation

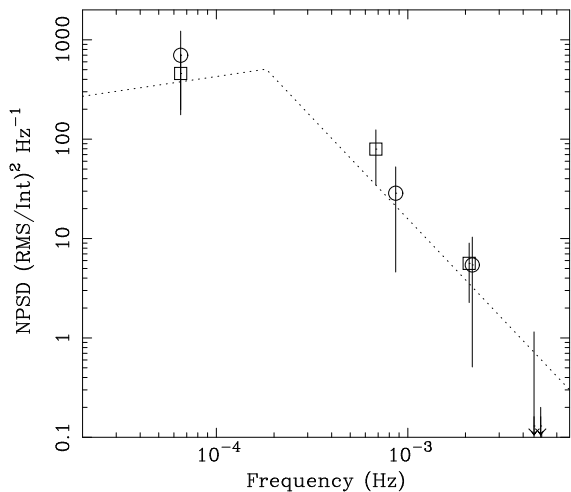


Figure 3. The normalized power spectrum density (NPSD) obtained from the SIS (open squares) and GIS (open circles) light curves. See Hayashida et al (1998) for the definition of the NPSD and the details of the computing method. Poisson noise has been subtracted. Negative values are found for both detectors at the highest frequencies (-1.03 ± 2.18 at 4.56×10^{-3} Hz for the SIS and -2.13 ± 1.87 at 4.94×10^{-3} Hz for the GIS) where the Poisson noise overwhelms the signal. The dotted line is the broken power-law fitted to the data, using the shape of the NPSD for NGC4051 (see Section 6.3 for details).

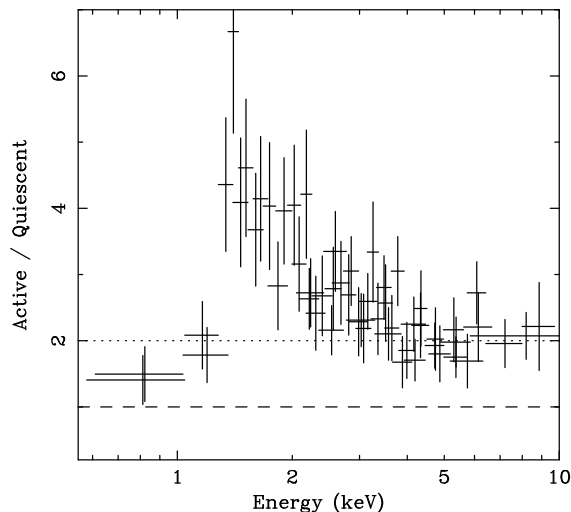


Figure 4. Spectral ratio of the data from the active state to the quiescent state. The small aperture SIS data and the GIS data above 2 keV are plotted. The dashed line indicates a ratio of unity while the dotted line shows a factor of two change which is consistent above 3 keV.

between the two states above 3 keV while a large excess variation is evident in the 1–2 keV band.

The X-ray source shows a rapid, large amplitude flux variations even within the active state. We next investigated spectral variability associated with the rapid flux variations, using a normalized count rate diagram (Fig. 5), similar to that used in Papadakis & Lawrence (1995) for NGC4051.

The whole 2–10 keV light curves of the S0 and S1 detectors were divided into six and four count-rate slices, respectively. Count rates from each slice in the 1–2 keV and 2.4–8

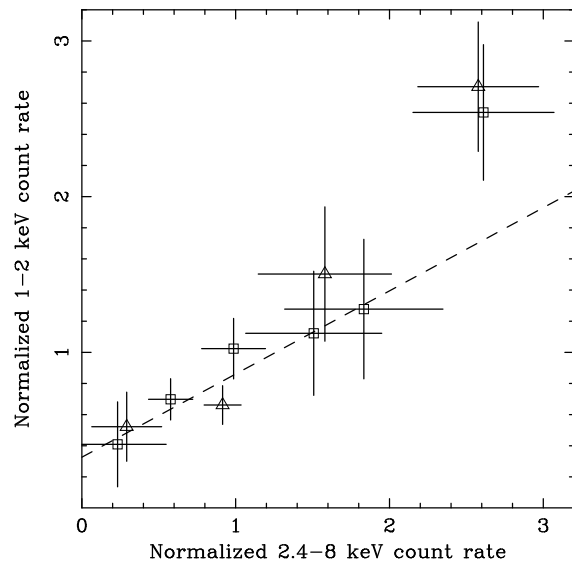


Figure 5. Plot of normalized count rates in the 1–2 keV band against those in the 2.4–8 keV band obtained from the S0 and S1 detectors for the six (S0; squares) and four (S1; triangles) count-rate slices, respectively, taken from each 2–10 keV light curve with 128 s bins. The dashed line shows the best-fit correlation for the data points, excluding the highest flux bins.

keV bands were then normalized by the mean count rates in the respective energy band. This plot could, in principle, track spectral variability on a time scale down to the time resolution of the light curve, 128 s. As Fig. 5 shows, a significant excess variation in the 1–2 keV band occurs at the highest flux bin. Since this bin contains all the three flare-peaks in the active state, the spectral softening appears to be associated with the flaring and may track it with a time lag of less than 10^3 s.

5 X-RAY SPECTRUM

As the image analysis shows, the X-ray spectrum of the nucleus of NGC4395 is hard, probably due to absorption. We first investigate the 2–10 keV data to determine the power-law continuum. Since the contamination from the nearby sources is negligible in this energy band, the large aperture data from both SIS and GIS integrated over the whole observation are used (Section 5.1).

On investigating the lower energy part of the spectrum, we use only the small aperture data from the SIS to avoid the contamination. A simple absorbed power-law model fails to explain the soft X-ray data due to the presence of excess emission. The soft excess emission is associated with the NGC4395 nucleus itself and possible origins are discussed (Section 5.2).

The low energy band spectrum shows a dramatic change during the active state (see Section 4.2). We examine the spectra during the quiescent and active states and try to explain the spectral change between the two states with a variable warm absorber model (Section 5.3).

The spectral analysis presented here was performed using XSPEC version 10.0. Quoted errors on spectral param-

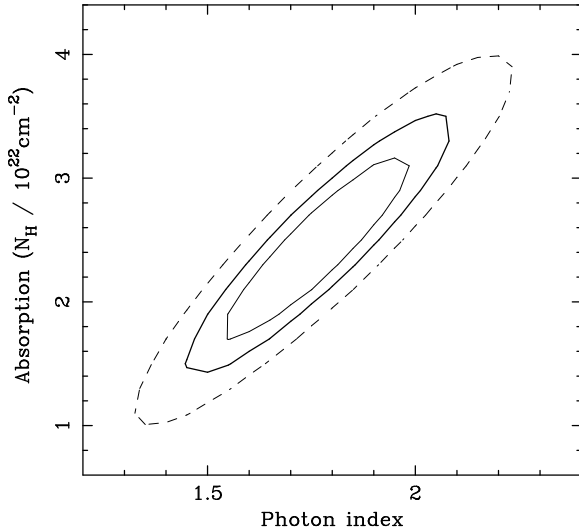


Figure 6. Confidence contours in the plane of photon-index against absorption column density obtained from a power-law fit to the total, time-averaged 2–10 keV data from the four detectors. The absorption is assumed to occur in neutral gas. The contours are drawn at the 68, 90 and 99 per cent confidence levels for two parameters of interest.

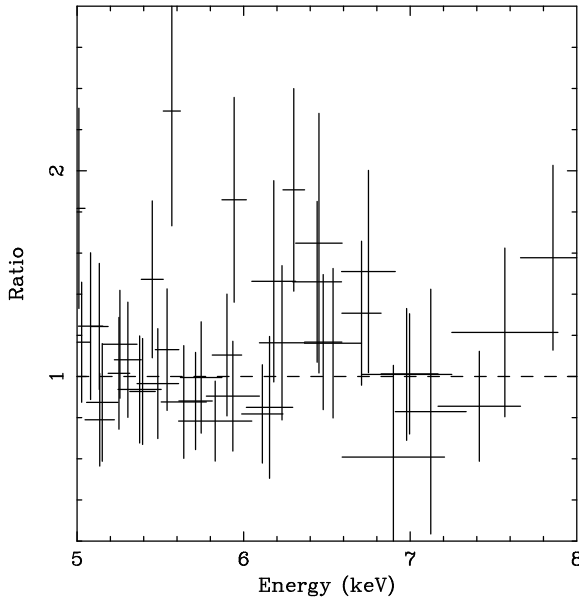


Figure 7. The ASCA SIS and GIS data of NGC4395 at the Fe K band divided by the best-fit power-law model for the neighbouring continuum. A Fe K line is detected at 6.45 keV marginally above the 90 per cent confidence level.

eters are 90 per cent confidence region for one parameter of interest, unless stated otherwise.

5.1 Time-averaged 2–10 keV spectrum

Fitting jointly the 2–10 keV data from the SIS and GIS with an absorbed power-law gives a photon-index $\Gamma = 1.72^{+0.24}_{-0.27}$ and column density $N_{\text{H}} = 2.3^{+0.8}_{-0.9} \times 10^{22} \text{cm}^{-2}$ (see confidence contours in Fig. 6). Here the absorption is assumed to be neutral and the absorption cross-sections taken from

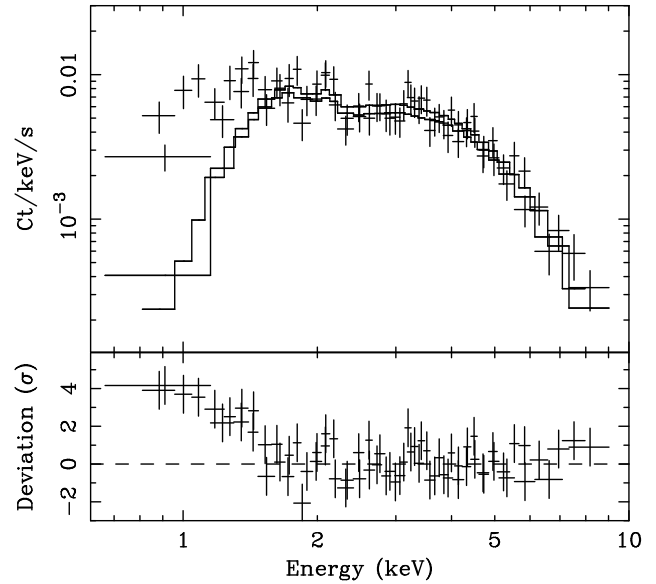


Figure 8. Upper panel: the time-averaged small-aperture spectrum of NGC4395 obtained from the ASCA SIS; lower panel: residuals in σ when the data are compared with the absorbed power-law model best-fitting the large-aperture 2–10 keV data ($\Gamma = 1.72$, $N_{\text{H}} = 2.3 \times 10^{22} \text{cm}^{-2}$) indicated in solid histograms in the upper panel. Surplus emission in the soft X-ray band is evident.

Morrison & McCammon (1983) are used. The higher energy continuum may be slightly steeper, e.g., $\Gamma = 2.1 \pm 0.3$ for the 4.5–10 keV data when N_{H} is fixed at $2.3 \times 10^{22} \text{cm}^{-2}$. A narrow iron K line is marginally detected at $6.45^{+0.28}_{-0.23}$ keV with an equivalent width (EW) of 180 ± 150 eV (Fig. 7). The observed 2–10 keV flux is $4.5 \times 10^{-12} \text{erg cm}^{-2} \text{s}^{-1}$, and the absorption-corrected 2–10 keV luminosity is $4.1 \times 10^{39} (D/2.6 \text{Mpc})^2 \text{erg s}^{-1}$, where D is the distance to the galaxy.

5.2 Variable soft X-ray spectrum and its possible origins

An extrapolation of the model best-fitting the 2–10 keV data to the lower energy leaves significant surplus emission below 2 keV (in the small aperture data, Fig. 8).

Here we discuss several possibilities for the origin of the excess soft X-ray emission. Thermal emission or reflected light of the obscured active nucleus from an extended region are readily ruled out by the rapid variability observed in the 1–2 keV band.

It could be a soft excess component intrinsic to the primary source like the one seen in the X-ray spectrum of Seyfert 1 galaxies and quasars and obscured by the same matter which attenuates the primary power-law. Assuming the soft excess has a blackbody type spectral form, a fit to the small-aperture spectrum together with the power-law sharing the same absorption ($N_{\text{H}} \sim 2 \times 10^{22} \text{cm}^{-2}$) suggests the blackbody to have a temperature $kT = 0.08 \pm 0.02$ keV. However, such obscured blackbody emission is argued against by the energetics. The soft X-ray luminosity of the blackbody component would be $3 \times 10^{42} \text{erg s}^{-1}$, when corrected for absorption, and 3 orders of magnitude above

the power-law component. It would produce far more luminous optical/UV emission-lines and far-infrared dust reradiation emission than observed.

Reflection from a partially ionized accretion disk could emerge in this energy range. However, the soft X-ray variation which is larger than that of the primary continuum is hard to explain by this hypothesis.

A possible solution is to introduce a warm absorber which varies in response to the continuum source. This model needs no extra X-ray source but does need different physical conditions for the X-ray absorber. Unlike many higher luminosity Seyfert 1 galaxies in which OVII (0.74 keV) and OVII (0.85 keV) are major features of the warm absorption, the primary absorption occurs around 2 keV in NGC4395. It requires a higher ionization parameter and the absorption is due to highly ionized O, Ne, Mg, Si, S and Fe-L.

Introducing a warm absorber reduces the opacity of the cold absorption significantly. This is more consistent with the observed optical/UV properties, e.g., non-stellar UV continuum, broad permitted line emission, high excitation lines usually seen in Seyfert 1 nuclei. The column density implied from cold absorption alone fitted to the 2–10 keV spectrum corresponds to $A_V \sim 10$ when the Galactic gas-to-dust ratio is used. The Seyfert-1 like optical/UV properties would not be observed if the central source and the broad-line region (BLR) are behind such a heavy obscuration, although some reddening to the BLR and the central source is still required given the ionizing photon deficit (e.g., for narrow H β), pointed out by Lira et al (1999), Kraemer et al (1999) and Moran et al (1999), the Seyfert 1.8/1.9 nature in the optical emission-line spectrum (e.g., Ho et al 1997) and the large H α /H β ratio (~ 5.1 , Kraemer et al 1999) for the broad component.

As the soft X-ray part of the spectrum has such a variable nature, a spectral variability study is more useful in modelling the soft X-ray spectrum than using the time-averaged spectrum alone. The warm absorber hypothesis is then explored to account for the spectral variability between the active and quiescent states in the next section.

5.3 Variable warm absorber

We try to model the spectral change in the soft X-ray band between the quiescent and active states with a warm absorber. The continuum source is assumed to have a constant spectral shape of a power-law with photon-index $\Gamma = 1.72$, obtained from the integrated 2–10 keV data, but different luminosities in the two states. Since it is unlikely that column density changes in response to the continuum source, the ionization parameter, $\xi = L/(nR^2)$ of absorbing matter is a primary driver of the spectral change. We used the warm absorber model `absori` by Done et al (1992) in XSPEC. Cold absorption is also included in the model. The small aperture SIS spectra of the quiescent and active states are fitted jointly to obtain parameters which are shared between the two datasets, such as a column density of an absorber. The mean absorption-corrected 2–10 keV fluxes of the power-law continuum during the quiescent and active states are $3.2 \times 10^{-12} \text{ erg cm}^{-2} \text{ s}^{-1}$ and $6.1 \times 10^{-12} \text{ erg cm}^{-2} \text{ s}^{-1}$, respectively.

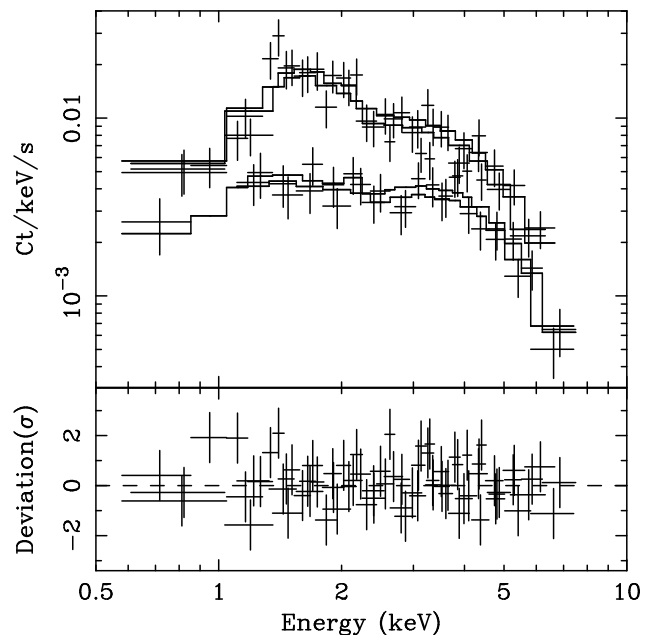


Figure 9. The ASCA SIS spectra of NGC4395 in the active (above) and quiescent (below) states fitted jointly with the multi-zone warm absorber model (Table 3). The contour levels are 68 and 90 per cent confidence regions for two parameters of interest. The ionization parameter of the variable absorber changes between the active and quiescent datasets in response to the continuum luminosity variation while the column density is assumed to remain the same. The constant absorber is common to the two datasets.

5.3.1 Single warm absorber model

A model of a single warm absorber with variable ξ plus a constant cold absorber is first fitted. The temperature of the absorbing gas is assumed to be 3×10^5 K. Column densities of warm and cold absorbers (N_W and N_H , respectively) are free parameters but set to vary in unison between the two datasets. The ionization parameter (ξ) of the absorber is allowed to take different values in the two datasets as well as the normalization of power-law. This parameter setting enables the model to accommodate a physically reasonable change in parameters in a variable warm absorber hypothesis. This model, however, gives a poor fit to the absorption band (below 2 keV). Despite the flux change of more than a factor of two, the ionization parameters obtained from the fit differ very little (Model-1 in Table 2).

When the values of N_W for the two datasets are also allowed to vary independently, the fit improved significantly (Model-2 in Table 2). However, not only has N_W decreased in the active state, but the lower ξ in the active state is in the opposite sense to the photoionization hypothesis. Therefore the single warm absorber model fails, but the latter fit instead suggests the existence of two physically distinct absorbers, i.e., the absorption feature in the two spectra are dominated by different absorbers. Next we try a multi-layer warm absorber model.

Table 2. Fits of the single warm absorber model to the quiescent and active state spectra. The photon-index of power-law, $\Gamma = 1.72$, is assumed for the two datasets. The warm absorber model **absori** (Done et al 1992) is used. The temperature of the absorber is assumed to be 3×10^5 K. Q and A denote the values for the quiescent and active state data, respectively. In Model (1), values for N_W are tied together between the two datasets while in Model (2), N_W are allowed to vary independently.

Model	T K	N_W 10^{22}cm^{-2}	ξ erg cm s^{-1}	N_H 10^{21}cm^{-2}	χ^2/dof
(1)	3×10^5	$7.0^{+1.7}_{-1.7}$	$Q: 92^{+17}_{-18}/A: 102^{+24}_{-22}$	$5.1^{+1.5}_{-1.1}$	75.63/67
(2)	3×10^5	$Q: 10.9^{+2.7}_{-2.3}/A: 2.5^{+1.1}_{-0.9}$	$Q: 109^{+18}_{-18}/A: 21^{+25}_{-15}$	$3.3^{+1.3}_{-0.9}$	50.42/66

Table 3. Multi-zone warm absorber fit to the quiescent and active state spectra. One absorber is assumed to be constant in both states while the other is variable only in ionization parameter (ξ_v). All the parameters of the two warm absorbers apart from ξ_v are shared between the two datasets. The photon-index of power-law, $\Gamma = 1.72$, is assumed. The temperatures of the absorbers are assumed to be 1×10^5 K for the constant absorber and 1×10^6 K for the variable one. Q and A denote the values for the quiescent and active state data, respectively.

T_c K	Constant			Variable		Cold N_H 10^{21}cm^{-2}	χ^2/dof
	N_W^c 10^{22}cm^{-2}	ξ_c erg cm s^{-1}	T_v K	N_W^v 10^{22}cm^{-2}	ξ_v erg cm s^{-1}		
1×10^5	$2.4^{+1.0}_{-0.7}$	31^{+36}_{-24}	1×10^6	$9.9^{+5.0}_{-4.0}$	$Q: 140^{+90}_{-45}/A: \geq 480$	$2.9^{+2.1}_{-2.8}$	55.75/65

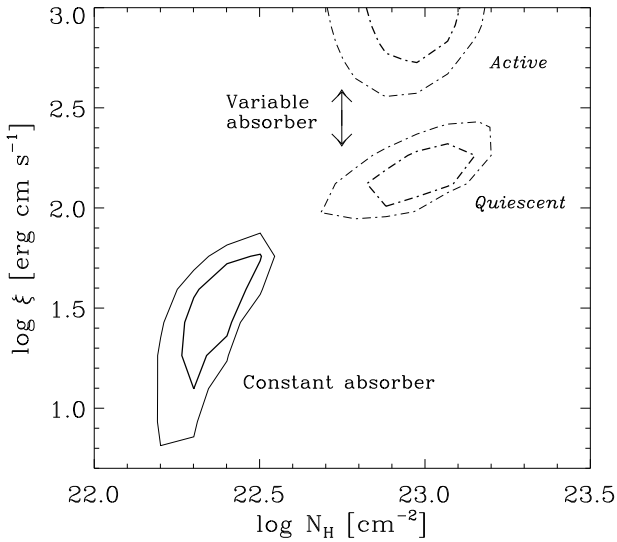


Figure 10. Confidence contours in the plane of column density (N_W) and ionization parameter (ξ) of the constant and variable warm absorbers when the multi-zone absorber model is fitted to the active and quiescent datasets jointly (see Table 4). The contour levels are 68 and 90 per cent confidence regions for two parameters of interest. The ionization parameter of the variable absorber changes between the active and quiescent datasets in response to the continuum luminosity variation while the column density is assumed to remain the same. The constant absorber is common to the two datasets.

5.3.2 Multi-zone warm absorber model

In addition to a variable warm absorber, a constant warm absorber, which is primarily seen in the active state, has been introduced. All the parameters of the two warm absorbers are shared by the two datasets apart from the ionization parameter of the variable absorber (ξ_v). The temperatures of the constant and variable absorbers are assumed to be 1×10^5 K and 1×10^6 K, respectively. This model gives

a good fit to the data despite the only one parameter (ξ_v) in the two warm-absorbers differing between the two datasets (Table 3, Fig. 9, Fig. 10).

The ionization parameter ($\xi_c \simeq 30 \text{ erg cm s}^{-1}$) and column density ($N_W^c \simeq 2 \times 10^{22} \text{cm}^{-2}$) of the constant absorber are found to be similar to those seen in higher luminosity Seyfert 1 nuclei (Reynolds 1997; George et al 1998). The variable absorber has a higher and variable ionization parameter (ξ_v) and a larger column density ($N_W^v \simeq 1 \times 10^{23} \text{cm}^{-2}$). It imposes an absorption feature above 1 keV and peaked around 1.5 keV in the quiescent state while it has almost disappeared in the active phase due to high ionization ($\xi_v \geq 480 \text{ erg cm s}^{-1}$). The change in ξ_v is marginally consistent with the change in luminosity of the continuum source which has shown a factor of 2–3 variations during the active phase. The multi-layer warm absorber model makes excess cold absorption marginally required at the 90 per cent significant level ($N_H = 2.8^{+2.1}_{-2.8} \times 10^{21} \text{cm}^{-2}$). The 0.5–2 keV fluxes for the quiescent and active states estimated from this model are $2.0 \times 10^{-13} \text{erg cm}^{-2} \text{s}^{-1}$ and $6.2 \times 10^{-13} \text{erg cm}^{-2} \text{s}^{-1}$, respectively. If the covering factor of the absorbing gas is high, emission-lines from the ionized gas in the absorber are expected. There is an emission-line like feature at 1.4 keV seen in the active state spectrum, which can be identified with MgXI.

6 DISCUSSION

6.1 Complex absorption in the nucleus of NGC4395

The 2–10 keV ASCA spectrum is well described by a power-law of $\Gamma \simeq 1.72$ modified by cold absorption of $N_H \simeq 2.3 \times 10^{22} \text{cm}^{-2}$. This cold absorption model however does not explain the soft X-ray spectrum (see Fig. 8). A variability study revealed that emission in the 1–2 keV band is more variable than in the higher energy band (Fig. 4). The variation above 2 keV is directly attributed to the intrinsic

flux change in the primary source. A plausible explanation for the excess variability in the 1–2 keV band is a change in a warm absorber.

Although Moran et al (1999) speculated about the presence of a warm absorber through spectral analysis of the ROSAT PSPC data, the properties of the X-ray absorption in NGC4395 appear to be more complex than they assumed. As shown by the ASCA spectrum, the ROSAT energy range is dominated by absorption, which makes the use of the PSPC spectrum to assess the primary continuum difficult.

A spectral fit to the ASCA data from the quiescent and active states can be explained by the presence of a constant and a variable warm absorber. The physical condition of the constant absorber is similar to that seen in many higher luminosity Seyfert 1 galaxies (Reynolds 1997; George et al 1998) while the variable absorber is found to have higher ionization parameter, which leads absorption features to be imprinted around 2 keV due to highly ionized O, Ne, Mg, Si, S and Fe-L. Evidence for multi-zone warm absorber has also been found in Seyfert 1 nuclei like MCG–6–30–15 (Otani et al 1996; Morales, Fabian & Reynolds 1999)

Using the formulae in Otani et al (1996) for the warm absorber in MCG–6–30–15, the recombination time scale for highly ionized gas can be approximated by $t_{\text{rec}} \simeq 200n_9^{-1}T_5^{0.7}(Z/Z_{\text{O}})^{-1}$ s, or $t_{\text{rec}} \simeq 200\xi_2L_{40}^{-1}T_5^{0.7}R_{-4}^2(Z/Z_{\text{O}})^{-1}$ s, where density is 10^9n_9 cm^{-3} , temperature is 10^5T_5 K, ionization parameter is $100\xi_2\text{ erg cm s}^{-1}$, the luminosity of the irradiating source is $10^{40}L_{40}\text{ erg s}^{-1}$, the distance of the warm absorber from the irradiating source is $10^{-4}R_{-4}$ pc, and Z is the atomic number ($Z_{\text{O}} = 8$ for oxygen). The luminosity of the continuum source during the active state is about $1 \times 10^{40}\text{ erg s}^{-1}$ at the source distance of 2.6 Mpc, when the power-law is integrated over 13.6 eV to 20 keV.

If the constant absorber, which is dominated by oxygen absorption, is indeed constant during the active state for 10^4 s, the recombination time scale is then $t_{\text{rec}}^c \geq 10^4$ s. This locates the absorber at the distance $R_c \geq 1.3 \times 10^{-3}L_{40}^{0.5}T_5^{-0.35}$ pc from the central source and constrains the density to be $n_c \leq 2 \times 10^7T_5^{0.7}\text{ cm}^{-3}$. On comparing with the model for the nuclear emission-line region derived from the photoionization calculation based on the optical/UV properties by Kraemer et al (1999), R_c is just outside the BLR (note that the size of the emission-line regions derived by Kraemer et al 1999 becomes larger if the ionizing luminosity obtained from our work is used). The absorption features seen across the CIV line profile presented in Kraemer et al (1999) could be due to this warm absorber, as the ionization parameter ($\xi \sim 30\text{ erg cm s}^{-1}$) is consistent with CIV.

The duration of the individual flares in the active state is about 1000 s. Since the spectral softening in the absorption band appears to occur at the peaks of those flares (Fig. 6), the recombination time scale of the variable absorber is probably less than the duration of the individual flares, i.e., $t_{\text{rec}}^v \leq 1000$ s. This gives constraints on density and distance of the absorber: $n_v \geq 10^9T_6^{0.7}(Z/Z_{\text{O}})^{-1}\text{ cm}^{-3}$, and $R_v \leq 4.5 \times 10^{-5}L_{40}^{0.5}T_6^{-0.35}(Z/Z_{\text{O}})^{0.5}$ pc, when the temperature of the absorber is $T_v = 10^6T_6$ K. As highly ionized Ne, Mg, Si and S as well as O are major elements for absorption, $(Z/Z_{\text{O}}) \simeq 1$ –2. The filling factor is described as $\Delta R/R = \xi N_{\text{W}}R/L \simeq 3 \times 10^{-2}\xi_2N_{\text{W}23}R_{-5}L_{40}^{-1}$,

where the distance of the absorber is $R = 10^{-5}R_{-5}$ pc and the column density is $N_{\text{W}} = 1 \times 10^{23}N_{\text{W}23}\text{ cm}^{-2}$. When $\xi_v = 500\text{ erg cm s}^{-1}$ and $R_v = 1 \times 10^{-5}$ pc are assumed, the filling factor and the density are $\Delta R/R \simeq 0.15$ and $n_v \simeq 2 \times 10^{10}\text{ cm}^{-3}$.

If the absorbing matter is space filling as suggested by the above argument, significant emission from the same matter is also expected. This is consistent with the detection of MgXI at 1.4 keV. Although the quality of our data is not sufficient to investigate weaker line emission, the emission could mask some absorption features which may cause a spuriously high ionization parameter.

6.2 Multi-wavelength energy distribution

It has been pointed out by Moran et al (1999, and also see Lira et al 1999) that the spectral energy distribution (SED) of NGC4395 diversifies from either a typical one of Seyfert/radio quiet quasars or of dwarf AGNs. In particular, X-ray quietness measured with ROSAT has been remarked. However, the absorption-corrected flux of the active nucleus in NGC4395 at 1 keV obtained from the present work is $\simeq 2.2 \times 10^{-12}\text{ erg cm}^{-2}\text{ s}^{-1}$, or $\simeq 1.7 \times 10^{39}(D/2.6\text{ Mpc})^2\text{ erg s}^{-1}$ in luminosity, an order of magnitude above the previous ROSAT estimates, which came from a measurement of the emission in the midst of the absorption band. The SED of NGC4395 over the radio to X-ray wave bands including our ASCA measurement is plotted in Fig. 11. Corrected for the absorption, the active nucleus in NGC4395 is no longer unusually X-ray quiet and the shape of the SED may be more similar to that of Seyferts or radio-quiet quasars than dwarf AGNs. The lack of an obvious “big blue bump” in the UV spectrum is still a major difference from higher luminosity Seyferts and quasars. This could be due to the small black hole mass inferred for this galaxy ($\sim 10^5M_{\odot}$, Kraemer et al 1999 and see the following section), which would shift the thermal emission peak from the accretion disk to shorter wavelengths thus it escapes being observed.

The UV–soft X-ray luminosity (10^{40} – $10^{41}\text{ erg s}^{-1}$), larger than previously estimated when corrected for the obscuration implied from the X-ray absorption, solves the problem of the ionizing photon deficit for the optical narrow lines and thus supports the hypothesis of a dust obscuration of the optical nucleus (Kraemer et al 1999). Part of the infrared emission detected by IRAS ($L_{\text{FIR}} \sim 1 \times 10^{41}\text{ erg s}^{-1}$) can be attributed to dust-reradiation of the absorbed soft X-ray and UV photons, although the cold IRAS colour ($S_{60}/S_{25} = 11.6$, $S_{100}/S_{60} = 2.7$) suggests that much of the infrared emission is due to the galaxy disk (Lira et al 1999).

6.3 X-ray variability and the black hole mass

Strong X-ray flux variation was observed during the present ASCA observation. This is consistent with an accreting black hole model to account for the nuclear activity in NGC4395 (Filippenko, Ho & Sargent 1993) and strongly argues against other hypotheses like a starburst. The large amplitude flux changes on a short time scale seen in NGC4395 is not typical of low luminosity AGN (Ptak et al 1998). The normalized excess variance obtained from this observation

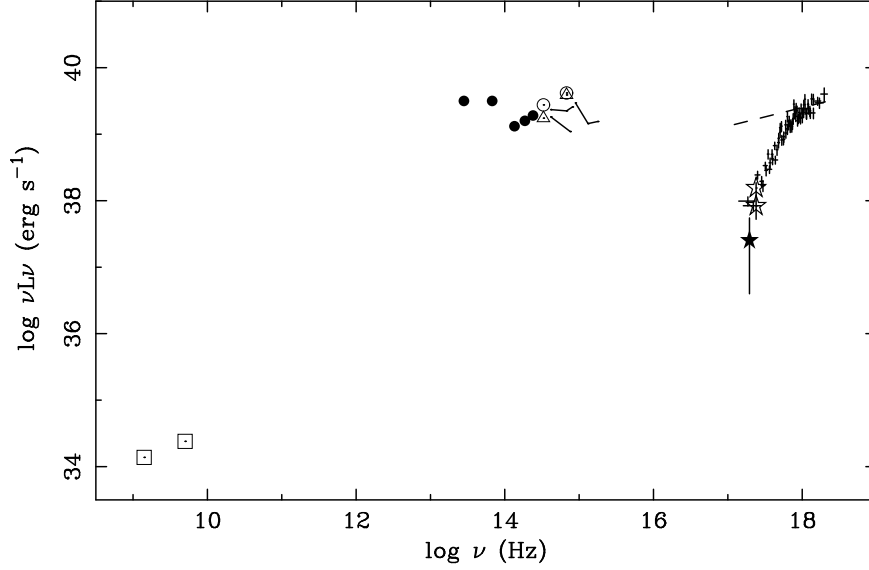


Figure 11. The spectral energy distribution of the nuclear source in NGC4395. The luminosities are calculated for a source distance of 2.6 Mpc. The data are compiled from Lira et al 1999 (solid lines, open circles and open triangles: optical/UV data from WHT and HST, details therein; open stars: ROSAT PSPC; filled star: ROSAT HRI) and Moran et al 1999 (open squared: VLA at 6cm and 20cm; solid circles: ISO/SWS, see also Kraemer et al 1999, and J, H, and K from Keck-I). The ASCA SIS 0.5–10 keV data are shown in crosses. The dashed line shows the unabsorbed power-law of $\Gamma = 1.7$. This demonstrates that the intrinsic soft X-ray luminosity of the nuclear source is actually an order of magnitude larger than that estimated from the ROSAT observations (Kraemer et al 1999; Lira et al 1999; Moran et al 1999).

is $\sigma_{\text{RMS}}^2 \simeq 0.2 \pm 0.07$, far above those for the sample of Ptak et al (1998).

The present observation of NGC4395 was only half-day long whereas typical observing time for the Seyfert galaxies in Nandra et al (1997) and dwarf AGN in Ptak et al (1998) is one-day. Correction for the observation length makes the σ_{RMS}^2 of NGC4395 larger by a factor of 1.4–2, depending on the power spectrum assumed (e.g., Lawrence & Papadakis 1993; Nandra et al 1997). Even without the correction, NGC4395 lies close to the extrapolation of the power-law fit to the σ_{RMS}^2 - $L_{2-10\text{keV}}$ relation (power-law index of ≈ -0.7) for their Seyfert-1 sample (Fig. 12). Although σ_{RMS}^2 for NGC4395 is slightly below the extrapolation, it could be consistent, given the uncertainty in extrapolating over five orders of magnitude. A flatter correlation $\sigma_{\text{RMS}}^2 \propto L_{2-10\text{keV}}^{-0.5}$ fits the sample of Nandra et al (1997) and NGC4395.

The mass of the black hole in NGC4395 has been estimated to be $\sim 10^5 M_{\odot}$ by various techniques (Lira et al 1999; Kraemer et al 1999; Filippenko & Ho 2000). Depending on the technique, it could be as large as few times $10^6 M_{\odot}$. The most tight constraint is available from a study of stellar kinematics, which provides the upper limit of $8 \times 10^4 M_{\odot}$ (Filippenko & Ho 2000). In any case, the light black hole mass is consistent with the small bulge of this galaxy (see the Introduction; e.g., Magorrian et al 1998).

We have tried to estimate the black hole mass in NGC4395 using the method employed by Hayashida et al (1998) who used X-ray variability as an estimator of a black hole mass in scaling that of the Galactic black hole binary Cyg X-1 whose black hole mass is assumed to be $10 M_{\odot}$. Note that the black hole masses of the AGNs analysed by Hayashida et al (1998) are generally one order of magnitude smaller than those estimated from optical broad line widths,

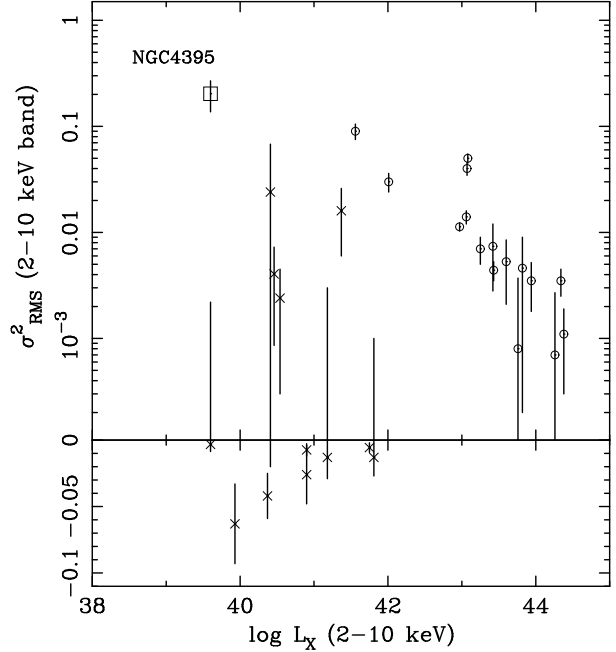


Figure 12. Plot of σ_{RMS}^2 against X-ray luminosity for the Seyfert 1 sample (open circles) of Nandra et al (1997), the dwarf AGN sample (crosses) of Ptak et al (1998) and NGC4395 (open square). Values of the normalized excess variance were computed for the 2–10 keV data and the X-ray luminosities are estimated in the 2–10 keV band corrected for absorption. The data point for NGC3079 is excluded because of the large error bar. Objects with positive σ_{RMS}^2 are plotted in the upper panel in log scale whilst those with a negative value are in the lower panel in linear scale.

broad-line reverberation, e.g., Wandel, Peterson & Malkan (1999). Therefore, this systematic error should be applied to the mass derived below. A detailed discussion on the reliability of the method, (i.e., the use of high frequency part of the NPSD instead of a “knee” frequency which has been found to change in Galactic black hole binary sources, e.g., Belloni & Hasinger 1990 for Cyg X-1, as a mass estimator) is found in Hayashida et al (1998).

Since the quality of the NPSD for NGC4395 is poor, we assume that it has a broken power-law form, which is canonical for AGN, with power-law indices obtained for NGC4051 (see Hayashida et al 1998) and that the normalization (N) follows $1/f$ scaling law. The only free parameter is the break frequency (f_b). We thus describe the NPSD for NGC4395 as

$$P(f) = \begin{cases} N(N4051)(f_b(N4051)/f_b)(f/f_b)^{+0.28} & (f < f_b) \\ N(N4051)(f_b(N4051)/f_b)(f/f_b)^{-2.01} & (f \geq f_b) \end{cases}$$

where $N(N4051) = 1.62 \times 10^3$ and $f_b(N4051) = 5.69 \times 10^{-5}$ Hz are the normalization and the break frequency for NGC4051. Fitting the f_b to the NPSD shown in Fig. 3 gives $f_b = 1.82_{-0.78}^{+1.64} \times 10^{-4}$ Hz with $\chi^2 = 4.90$ for 7 degrees of freedom. The scaling from $M_{\text{BH}}(N4051)$ (see Fig. 4 in Hayashida et al 1998) then yields $2.8_{-1.8}^{+2.4} \times 10^4 M_{\odot}$ for the black hole mass in NGC4395 (the systematic error associated with this method and the limitation due to our assumption of the shape of NPSD should be noted, as mentioned above).

The normalized excess variance of NGC4395 ($\sigma_{\text{RMS}}^2 \simeq 0.2$) is larger than NGC4051 ($\sigma_{\text{RMS}}^2 \simeq 0.1$, Nandra et al 1997) by a factor of 2. As noted in Nandra et al (1997) and Papadakis & Lawrence (1993), σ_{RMS}^2 should be proportional to the power at a given frequency, if the sampling and power spectra are similar between the sources. The power spectrum of NGC4395 could therefore be approximated by multiplying the one for NGC4051 by 2. This leads to a NPSD which agrees with the result obtained above.

Although many assumptions are involved, the black hole mass in NGC4395 implied from the X-ray variability is $\sim 3 \times 10^4 M_{\odot}$, with an uncertainty of up to a factor of ten. This is consistent with the upper limit obtained from the stellar kinematics by Filippenko & Ho (1999) and, together with the other estimates, points to a relatively light mass black hole. If NGC4395 harbours a black hole of order of $10^5 M_{\odot}$ or less, and the scaling law indeed operates, the low-frequency break, or “knee”, in the power spectrum, seen in some Galactic black hole sources and AGN (Belloni & Hasinger 1990; Hayashida et al 1998; Edelson & Nandra 1999), to be seen around 10^{-4} Hz or higher frequencies as suggested by the fit presented above (this is however subject to the stability of the break frequency at a given black hole mass). In order to test this prediction, a longer continuous observations is needed. However, unlike higher luminosity AGN, a modest length (say, one-day) observation will suffice. The rapid X-ray variability together with accompanying spectral change makes NGC4395 an ideal target for XMM.

The Eddington luminosity for a $10^5 M_5 M_{\odot}$ black hole is $L_{\text{Edd}} \simeq 1.3 \times 10^{43} M_5 \text{ erg s}^{-1}$. The ratio of the 2–10 keV and bolometric luminosities is typically a few per cent for QSOs and ~ 10 per cent for Seyfert galaxies (e.g., Elvis et al 1994). The bolometric luminosity of NGC4395 may therefore be in the range of 10^{40} – 10^{41} erg s^{-1} . The Eddington ratio is thus $L_{\text{Bol}}/L_{\text{Edd}} = 6 \times 10^{-3} M_5^{-1} (f_{\text{HX} \rightarrow \text{Bol}}/20)$, where $f_{\text{HX} \rightarrow \text{Bol}}$ is

the bolometric correction factor for the 2–10 keV luminosity. If M_5 is about unity or smaller, the Eddington ratio would be in a range of ordinary Seyfert 1 nuclei. On the other hand, if M_5 is significantly larger than 10, the ratio would be in the ADAF range (e.g., Kato, Fukue & Mineshige 1998). Since the observed rapid X-ray variability does not fit the ADAF model, a light black hole ($M_5 < 1$) is favoured.

The apparent small black hole mass of NGC4395 suggests that X-ray variability in AGN correlates with black hole mass, not directly with luminosity. This may argue that most dwarf AGN like the sample galaxies in Ptak et al (1998) have massive black holes with low accretion rates.

ACKNOWLEDGEMENTS

We thank the ASCA team for their efforts on operation of the satellite, and the calibration and maintenance of the software. The ROSAT data were obtained through the High Energy Astrophysics Science Archive Research Center (HEASARC), provided by NASA’s Goddard Space Flight Center. ACF and KI thank the Royal Society and PPARC for support, respectively.

REFERENCES

- Barth A.J., Filippenko A.V., Moran E.C., 1999, ApJ, 525, 673
 Belloni T., Hasinger G., 1990, A&A, 227, L33
 Condon J.J., Cotton W.D., Greisen E.W., Yin Q.F., Perley R.A., Taylor G.B., Broderick J.J., 1998, AJ, 115, 1693
 Dickey J.M., Lockman F.J., 1990, ARAA, 1990, 28, 215
 Done C., Mulchaey J.S., Mushotzky R.F., Arnaud K.A., 1992, ApJ, 395, 275
 Edelson R., Nandra K., 1999, ApJ, 514, 682
 Elvis M., et al, 1994, ApJS, 95, 1
 Fabian A.C., Rees, M.J., 1995, MNRAS, 277, L55
 Filippenko A.V., Sargent W.L.W., 1989, ApJ, 342, L11
 Filippenko A.V., Ho L.C., Sargent W.L.W., 1993, ApJ, 410, L75
 Filippenko A.V., Ho L.C., 2000, ApJ, submitted
 George I.M., Turner T.J., Netzer H., Nandra K., Mushotzky R.F., Yaqoob T., 1998, ApJS, 114, 73
 Griffiths R.E., Padovani P., 1990, ApJ, 360, 483
 Guainazzi M., et al, 1998, MNRAS, 301, L1
 Hayashida K., Miyamoto S., Kitamoto S., Negoro H., 1998, ApJ, 500, 642
 Heckman T.M., 1980, A&A, 87, 152
 Heckman T.M., Armus L., Miley G.K., 1990, ApJS, 74, 833
 Ho L., Filippenko A.V., Sargent W.L.W., 1997a, ApJS, 112, 315
 Ho L., Filippenko A.V., Sargent W.L.W., 1997b, ApJS, 112, 391
 Iwasawa K., 1999, MNRAS, 302, 96
 Kato S., Fukue J., Mineshige S., 1998, Black Hole Accretion Disks, Kyoto: Kyoto University Press
 Kormendy J., Richstone D., 1995, ARAA, 33, 581
 Kraemer S.B., Ho L.C., Crenshaw D.M., Shields J.C., Filippenko A.V., 1999, ApJ, 520, 564
 Lawrence A., Papadakis I.E., 1993, ApJ, 414, L85
 Lira P., Lawrence A., O’Brien P., Johnson R.A., Terlevich R., Bannister N., 1999, MNRAS, 305, 109
 Lomb N.R., 1976, Ap&SS, 39, 447
 Magorrian, J., et al. 1998, AJ, 115, 2285
 Morales R., Fabian A.C., Reynolds C.S., 2000, MNRAS, in press
 Moran E.C., Filippenko A.V., Ho L.C., Shields J.C., Belloni T., Comastri A., Snowden S.L., Sramek R.A., 1999, PASP, 111, 801
 Morrison R., McCammon D., 1983, ApJ, 270, 119

- Nandra K., George I.M., Mushotzky R.F., Turner T.J., Yaqoob T., 1997, ApJ, 476, 70
Otani C., et al, 1996, PASJ, 48, 211
Ptak A., Yaqoob T., Mushotzky R., Serlemitsos, P., Griffiths R., 1998, ApJ, 501, L37
Radecke H.-D., 1997, A&A, 319, 18
Reynolds C.S., 1997, MNRAS, 286, 513
Richstone D., et al, 1998, Nat, 395, 14
Serlemitsos P.J., et al, 1995, PASJ, 47, 105
Terashima Y., 1998, PhD thesis, Nagoya University, Japan
Turner T.J., George I.M., Nandra K., Turcan D., 1999, ApJ, 524, 667
Wandel A., Peterson B.M., Malkan M.A., 1999, ApJ, 526, 579
Ward M.J., Done C., Fabian A.C., Tennant A.F., Shafer R.A., 1988, ApJ, 324, 767